J Fluoresc (2009) 19:495–500
DOI 10.1007/s10895-008-0438-7

ORIGINAL PAPER

Europium(III) Concentration Effect on the Spectroscopic and Photoluminescent Properties of $BaMoO_4$:Eu

Ieda L. V. Rosa · Ana Paula A. Marques · Marcos T. S. Tanaka · Fabiana V. Motta · José A. Varela · Edson R. Leite · Elson Longo

Received: 19 June 2008 / Accepted: 27 October 2008 / Published online: 11 November 2008

Abstract $BaMoO_4$:Eu (BEMO) powders were synthesized by the polymeric precursor method (PPM), heat treated at 800 °C for 2 h in a heating rate of 5 °C/min and characterized by powder X-ray diffraction patterns (XRD), Fourier Transform Infra-Red (FTIR) and Raman spectroscopy, besides room temperature Photoluminescence (PL) measurements. The emission spectra of BEMO samples under excitation of 394 nm present the characteristic Eu^{3+} transitions. The relative intensities of the Eu^{3+} emissions increase as the concentration of this ion increases from 0.01 to 0.075 mol, but the luminescence is drastically quenched for the $Ba_{0.855}Eu_{0.145}MoO_4$ sample. The one exponential decay curves of the Eu^{3+} $^5D_0 \rightarrow {}^7F_2$ transition, λ_{exc}=394 nm and λ_{em}=614 nm, provided the decay times of around 0.54 ms for all samples. It was observed a broadening of the Bragg reflections and Raman bands when the Eu^{+3} concentration increases as a consequence of a more disordered material. The presence of MoO_3 and $Eu_2Mo_2O_7$ as additional phases in the BEMO samples where observed when the Eu^{3+} concentration was 14.5 mol%.

Keywords Europium · Molybdate · Complex Polymerization Method · Photoluminescence

I. L. V. Rosa (✉) · A. P. A. Marques · M. T. S. Tanaka · F. V. Motta · E. R. Leite
LIEC-CMDMC, DQ, UFSCar,
Via Washington Luiz, km 235,
CEP 13565-905 São Carlos, SP, Brazil
e-mail: ilvrosa@power.ufscar.br

J. A. Varela · E. Longo
LIEC-CMDMC, IQ, UNESP,
Rua Francisco Degni s/n,
CEP 14800-900 Araraquara, SP, Brazil

Introduction

Phosphor-converted light-emitting diodes (LEDs) and tri-color phosphors are considered the next generation of solid state illumination materials since the first LED became commercially available in 1997 [1]. The current phosphor materials commercially available for solid state lighting are $Y_2O_2S:Eu^{3+}$ for red, ZnS:(Cu^+, Al^{3+}) for green, and $BaMgA_{l0}O_{17}:Eu^{2+}$ (BAM) for blue [2, 3]. They are now quite important for applications in cathode ray tubes and plasma display panels. The efficiency of the $Y_2O_2S:Eu^{3+}$, however, is low compared to the blue and green phosphor. Besides, the lifetime of this red phosphor is inadequate when ultraviolet irradiations of low energy are used. In this way phosphors that absorb in the near UV and emit in the red range of the electromagnetic spectra are still required. The search for a stable inorganic phosphor based on rare earth with a high absorption in the near ultraviolet or blue spectral region is consequently an attractive and challenging research assignment.

Europium in its trivalent state is one of the most studied through the luminescence spectroscopy among the rare earth ions as a consequence of the simplicity of its spectra and due of its wide application as red phosphor in color TV screens. This ion have also attracted significant attention of the researchers due to their potential application as biological sensors, phosphors, electroluminescent devices, optical amplifiers or lasers when it is used as doping in a variety of materials [4, 5]. Besides, the luminescence spectra of the Eu^{3+} presents emission lines extending from visible to near infrared with a relatively simple energy level structure. Especially the $^5D_0 \rightarrow {}^7F_J$ (J=0, 1, 2,…6) manifold enables one to ascertain the microscopic symmetry around the site, making the Eu^{3+} an ideal experimental probe of the crystalline environment [6, 7].

Molybdates are being considered as good hosts for luminescent materials due to its excellent thermal and chemical stability [8, 9]. In recent papers, calcium molybdate ($CaMoO_4$) phosphor doped with trivalent europium (Eu^{3+}) and terbium (Tb^{3+}) ions have been prepared through the Pechini method, and its luminescent properties were investigated under UV and X-ray excitation. According to the authors, these ions show high luminescent efficiency in emitting red and green light in single doped samples. In these materials the energy transfer from MoO_4^{2-} tetrahedron unit to Eu^{3+} and Tb^{3+} ions occurs only when the $CaMoO_4$ matrix is co-doped at low concentration with Eu^{3+} and Tb^{3+} ions. Energy transfer processes from the host to the activators besides the interaction between these activators were also observed when the lanthanide concentrations were higher than 1.5% [10]. However, there are few studies about the structural and optical properties of molybdates when it is doped with lanthanides. In this way in a previous work $Ba_{0.99}Eu_{0.01}MoO_4$ (BEMO:0.01) powders were prepared for the first time in our laboratory using the Complex Polymerization Method [11]. According to this study, BEMO:0.01 powders show the crystalline scheelite-type phase after the heat treatment at 400 °C. The PL emission of the BEMO:0.01 heat-treated in temperature higher that 700 °C presented a marked increase in its intensities compared to the same materials heat-treated in minor temperature. In this study it was also observed a decrease in the lattice parameters *a* and *c* of the Eu^{3+} doped samples compared to the matrix $BaMoO_4$. As the ionic radius of EuO_8 clusters (0.109 nm) is lower than of BaO_8 one (0.149 nm), this observation indicates that Eu^{3+} is located in the same tetragonal (S_4) symmetry as the Ba^{2+} sites does in the crystalline structure of $BaMoO_4$ matrix, demonstrating the replacement of some BaO_8 cluster for EuO_8. Since the preparation of molybdates powders by the conventional solid-state reaction method give rise to powders with large grain size and irregular morphology and it is also necessary the use of high annealing temperature and long reaction time, the Complex Polymerization Method (CPM) was used to prepare pure and Eu^{3+} doped $BaMoO_4$ powders in this current study. This method allows the use of low annealing temperature and reduces the metal segregation, which promotes the compositional homogeneity at the molecular scale. These advantages permit the cation distribution and promote the chemical homogeneity throughout the gel system, which determines the compositional homogeneity of the material in the multi-component oxides [12, 13].

The study on the photophysical properties of Eu^{3+} doped $BaMoO_4$ matrix has continued in this work to obtain a better comprehension of the material when different concentrations of this ion are used. The obtained $Ba_{1-x}Eu_xMoO_4$ powders (BEMO), where x=0.0; 0.01; 0.03; 0.05; 0.075 and 0.145, were synthesized by CPM, heat treated from 800 °C for 2 h in a heating rate of 5 °C/min and characterized by powder X-ray diffraction patterns (XRD), Fourier Transform Infrared (FTIR) and Raman spectroscopy, besides room temperature Photoluminescence (PL) measurements.

Experimental

Preparation of $Ba_{1-x}Eu_xMoO_4$ (BEMO) powders

The chemical reagents used in this study without further purification were molybdenum trioxide MoO_3 (Synth 85%), $BaCO_3$, (Mallinckrodt 99%), europium (III) oxide (Aldrich, USA, 99.999%), citric acid ($H_3C_6H_5O_7$) (Mallinckrodt 99%) and ethylene glycol ($HOCH_2CH_2OH$) (J. T. Baker 99%).

$Ba_{1-x}Eu_xMoO_4$ powders (x=0.0; 0.01; 0.03; 0.05; 0.075 and 0.145), were produced by CPM as already described in a previous work [11]. In this study the molar ratio between Ba^{+2} and Eu^{+3} it was set in the respective proportions of 100:0, 99:1, 97:3, 95:5, 92.5:7.5 and 85.5:14.5. The obtained dark-brown powders were deagglomerated using a mortar and were finally annealed at 800 °C for 2 h under ambient atmosphere using a heating rate of 5 °C/min, giving rise to white powders with the respective amount of Eu^{3+} ions denoted as BEMO.

Characterizations

The structural evaluation and the unit cell volume of the BEMO powders were determined through its X-ray diffraction patterns (XRD) using a Rigaku Dmax2500PC diffractometer. The average crystallite diameter (Dcrys) of the materials after the heat treatment was determined using the (112) diffraction peak of the $BaMoO_4$ phase, which 2θ is located at around 26.5°, using the procedure described elsewhere [14].

Fourier transform infrared (FTIR) spectra were obtained in an Equinox/55 Bruker spectrometer, while Raman spectroscopy data were obtained in a RFS/100/S Bruker FT-Raman equipment. The room temperature photoluminescence (PL) data of the BEMO powders were obtained in a Jobin Yvon-Fluorolog spectrofluorometer using a 450 W xenon lamp as excitation energy source. Luminescence lifetime measurements were carried out as well using a 1934D model spectrophosphorometer coupled to the spectrofluorometer.

Results and discussion

The CPM utilized to prepare the $Ba_{1-x}Eu_xMoO_4$ (BEMO) powders, where x=0.0, 0.01, 0.03, 0.05, 0.075 and 0.145, was efficient to obtain these materials in a small size grains

and high morphological homogeneity, properties which are not so ease to be obtained when the solid state reaction method is employed.

Figure 1 shows the XRD patterns of the BEMO powders heat treated at 800 °C for 2 h in a heating rate of 5 °C/min. According to these data the samples present a crystalline scheelite-type phase, which was indexed to the JCPDS data base no 29-0193. The presence of MoO_3 and $Eu_2Mo_2O_7$ indexed respectively through the JCPDS no 37-1445 and no 22-1098 were observed as additional phases only in the $Ba_{0.855}Eu_{0.145}MoO_4$ sample, with the larger percentage of Eu^{3+} in the doped materials (Fig. 1 f). Table 1 presents the cell volumes and lattice constants of the tetragonal structure of the BEMO samples. The calculated values of the cell volumes decrease as the Eu^{3+} concentration improves. The lattice parameters *a* and *c* were determined using the least square refinement from the REDE93 program and were obtained from the peak positions displayed in Fig. 1. It was observed a decrease in these values as the Eu^{+3} content increases, especially for the $Ba_{0.855}Eu_{0.145}MoO_4$ sample, where a=5.567 (1) and c=12.785 (5).

The replacements of the BaO_8 clusters for EuO_8 ones, which are framework modifiers, give rise to vacancies into the MoO_4^{2-} clusters, which are lattice former, produced because the europium ion has a charge greater than the barium one, promoting the appearing of a more quantity of defects (vacancies) in the doped material. It is expected also in this case that Eu^{3+} presents the same Ba^{2+} symmetry ascribed to S_4.

Spontaneous Raman spectra are presented in Fig. 2. The primitive cell of $BaMoO_4$ includes two formula units, according to Basiev [15]. The scheelite primitive cell presents 26 different vibrational modes including Γ_{Td}= $3A_g + 5A_u + 5B_g + 3B_u + 5E_g + 5E_u$, but only the A_g, B_g and E_g ones are Raman-active [15].

Table 1 Lattice constants (Å) and cell volumes ($Å^3$) of the tetragonal structure of $Ba_{1-x}Eu_xMoO_4$ powders, where x=0.00, 0.01, 0.03, 0.05, 0.075 and 0.145, prepared by the CPM method and heat treated at 800 °C for 2 h

$Ba_{1-x}Eu_xMoO_4$	Lattice constants (Å)		Cell volumes ($Å^3$)
	A	*c*	
x=0	5.579 (1)	12.811 (4)	399
x=0.01	5.579 (0.3)	12.816 (1)	399
x=0.03	5.571 (1)	12.791 (4)	397
x=0.05	5.571 (1)	12.790 (6)	397
x=0.075	5.565 (2)	12.748 (10)	395
x=0.145	5.567 (1)	12.785 (5)	396

Raman spectroscopy is an effective tool for studying the effects of structural disorder. For a perfect crystal, the first-order Raman phonon spectrum consists of narrow lines that correspond to Raman-allowed zone center (Γ-point) modes, which obey definite polarization selection rules. For the case of disordered crystals, however, the following features are anticipated in the phonon spectrum: (i) a broadening of the first-order Raman lines; (ii) the activation of forbidden Raman phonons; (iii) appearance of broad Raman bands reflecting the phonon density of states; (iv) frequency shifting of some peaks proportional to the concentration of the dopant element (i.e., one-phonon-like behavior) and (v) splitting of some peaks involving different elements that share the same lattice site (i.e., two-phononlike behavior) [16]. As it is observed in Fig. 2, as the Eu^{+3} concentration increase, the bands in the Raman spectra became broader. This behavior is ascribed to a more intense structural disorder caused by the increase of the doped ion in the

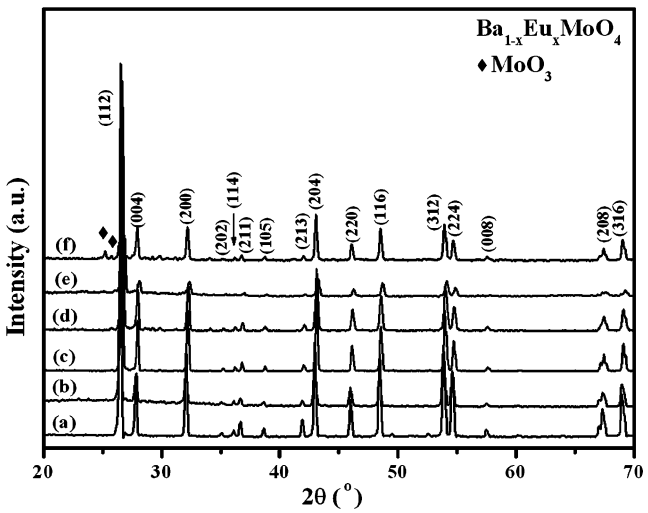

Fig. 1 X-ray diffraction patterns of $Ba_{1-x}Eu_xMoO_4$ powders, where x= *a* 0.00, *b* 0.01, *c* 0.03, *d* 0.05, *e* 0.075 and *f* 0.145 prepared by the CPM method and heat treated at 800 °C for 2 h

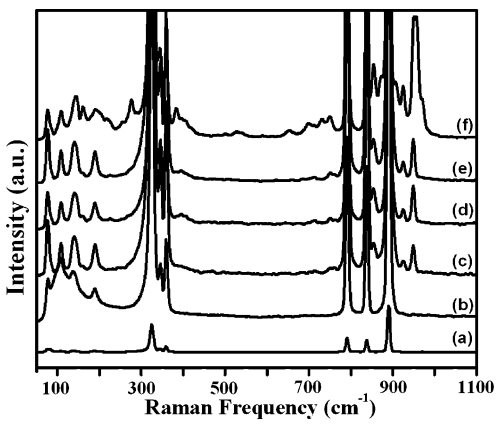

Fig. 2 Spontaneous Raman spectra of the $Ba_{1-x}Eu_xMoO_4$ powders heat tread at 800 °C for 2 h, where x= *a* 0.00, *b* 0.01, *c* 0.03, *d* 0.05, *e* 0.075 and *f* 0.145

material. The assignments of the Raman-active vibration modes of these materials are detailed in Table 2.

The BEMO powders heat treated at 800 °C for 2 h were crystalline, displaying scheelite-type phases in the DRX and Raman data. However, when the Eu^{+3} concentration increases, it was observed a broadening of the Bragg reflections and Raman bands. These observations demonstrate that the materials doped with a more concentration of europium present a higher degree of structural disorder than those without e/or with a minor concentration of this ion. Table 3 presents the calculated values of the full width at half maximum (FWHM) obtained with the Raman and XRD data. These values confirm the increase of the structural disorder as the Eu^{3+} concentration increases.

The scheelite-type crystalline structure presents in the FTIR spectra only the bands related to the $F_2(\nu_3, \nu_4)$ (B_g and E_g) modes. The $F_2(\nu_3)$ vibration is the antisymmetric stretch while the $F_2(\nu_4)$ is a bending mode. The spectra of the BEMO samples display a very broad absorption band from 810 to 830 cm^{-1}, assigned to the $F_2(\nu_3)$ antisymmetric stretch, related to the Mo–O stretching vibration in the MoO_4^{2-} tetrahedral [17].

Figure 3 (a–d) presents the room-temperature excitation spectra of BEMO, which were obtained setting the Eu^{3+} emission maximum at 614 nm. In these spectra it is noticed as the main peak the Eu^{3+} characteristic excitation band related to the $^5L_6$ transition located at 394 nm. The presence of a broad band is ascribed to the charge-transfer intra-configurational transition of the MoO_4^{2-} unit with the maximum at around 290 nm. The increase in the intensities of both excitation bands as the Eu^{3+} concentration increases from 0.01 to 0.075 mol was also observed. However, when the Eu^{3+} concentration is higher than 0.075 mol, the intensities of these bands follow drastically as it is seen for the sample having 0.145 mol of this ion (Fig. 3 d).

Table 3 Full width at half maximum (FWHM) obtained through the Raman and XRD data of the BEMO powders

$Ba_{1-x}Eu_xMoO4$	Raman peak at 891 cm^{-1}	XRD (112) diffraction peak (2θ around 26.5)
x=0	5.82 (3)	0.171 (4)
x=0.01	6.03 (5)	0.177 (3)
x=0.03	5.94 (4)	0.140 (2)
x=0.05	6.03 (6)	0.173 (3)
x=0.075	6.10 (6)	0.217 (9)
x=0.145	6.13 (12)	0.153 (3)

Figure 4 shows the room-temperature emission spectra of BEMO powders heat-treated at 800 °C for 2 h. The emission spectra of these samples under 394 nm near-UV excitation are composed of groups of several sharp lines ascribed to the characteristic Eu^{3+} red emission. It was observed through these spectra that the relative intensity of the Eu^{3+} emissions increase as the concentration of this ion increases from 0.01 to 0.075 mol. However, when the Eu^{3+} concentration is higher than this value the intensities of the emission bands are quenched drastically, as it is seen for the sample with 0.145 mol (Fig. 4 d). This behavior indicates the presence of different energy transfer processes occurring in each situation. When the Eu^{3+} concentrations are smaller than 0.075 mol, the non-radiative mechanism of energy transfer between the Eu^{3+} ions is absent. It was observed however that the charge-transfer from the O 2p state to the Mo 4d state is present in this situation and increase as the Eu^{3+} concentration increases. The MoO_4^{2-} units make an important role absorbing the excitation energy and transfer it

Table 2 Raman mode frequencies in the $Ba_{1-x}Eu_xMoO_4$ powders, where x=0.00, 0.01, 0.03, 0.05, 0.075 and 0.145

Lattice mode symmetry C^6_{4h}	x values of $Ba_{1-x}Eu_xMoO_4$						Assignments
	0	0.01	0.03	0.05	0.075	0.145	
A_g	891	890	891	891	891	891	ν_1 (A_1)
B_g	838	838	837	837	837	837	ν_3 (F_2)
E_g	791	791	791	791	791	791	
E_g	359	359	359	359	359	359	ν_4 (F_2)
B_g	346	346	345	345	345	345	
B_g	326	325	324	324	324	324	ν_2 (E)
A_g	325	325	324	324	324	324	
E_g	190	190			189	191	$\nu_{f.r.}$ (F_1) free rotation
B_g	141	138	141	141	141	145	$\nu_{ext.}$—external Modes MoO^{2-}_4 and Ba^{2+} motions
E_g	107	108	108	108	108	108	
B_g	78	78	75	75	76	76	
E_g	76						

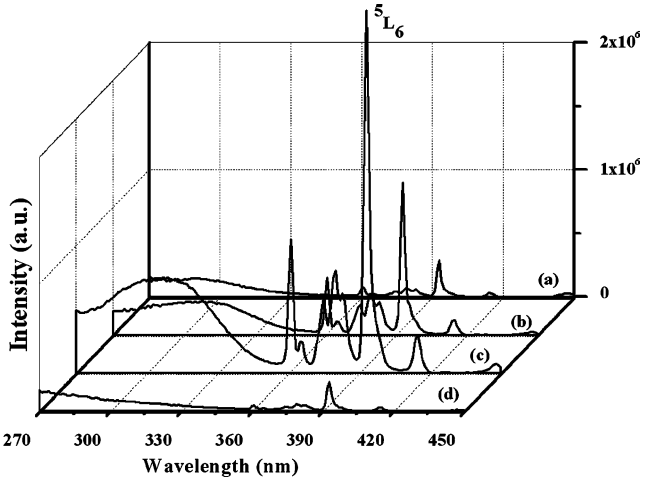

Fig. 3 Room-temperature excitation spectrum of $Ba_{1-x}Eu_xMoO_4$ powders, where x=*a* 0.01, *b* 0.03, *c* 0.075 and *d* 0.145, heat-treated at 800 °C for 2 h, when the emission is set at 614 nm

then to the Eu^{3+}. This process increases the population of the excited state of this ion and promotes the enhancement of its emission. The increase in the intensity of the broad band, located at around 290 nm (Fig. 3 c), is also ascribed to this phenomenon. Both of the described mechanisms contribute to the increase of the Eu^{3+} emission intensities. When the Eu^{3+} concentration is higher than 0.075 mol, however, the mechanism which prevails is the energy transfer from one Eu^{3+} ion to another. This energy migration process promotes an increase of the non-radiative relaxation, since the optical excitation is trapping at defects or impurity sites. In this way, the non-radiative transitions among different Eu^{3+} sites in the samples are responsible for the Eu^{3+} luminescence inhibition, the so called quenching concentration [18]. PL properties in a pure material are directly related to the degree of structural order-disorder [11, 19]. The appropriate structural disorder in a material can result in a better PL emission compared to a completely ordered one. Materials which are structurally disordered in general present oxygen vacancies, lattice defects, impurities and/or local bond distortions, which yield localized electronic levels in their band gap. These electronic levels are responsible for enhancing the PL emission processes.

The samples presented in their emission spectra (Fig. 4 a–d) the $^5D_1 \rightarrow {}^7F_0$, $^5D_1 \rightarrow {}^7F_1$ and $^5D_1 \rightarrow {}^7F_2$ transitions at 523, 533 and 554, respectively. Besides, it was also observed the $^5D_0 \rightarrow {}^7F_0$, $^5D_0 \rightarrow {}^7F_1$, $^5D_0 \rightarrow {}^7F_2$, $^5D_0 \rightarrow {}^7F_3$ and $^5D_0 \rightarrow {}^7F_4$ Eu^{3+} transitions at around 578, 589, 614, 652 and 699 nm, respectively. These groups of sharp emission bands can be better observed at Fig. 5, which show the emission spectra of the $Ba_{0.925}Eu_{0.075}MoO_4$ sample heat treated at 800 °C for 2 h under excitation of 394 nm. The emission spectrum are dominated by the peak at around 614 nm ascribed to the Eu^{3+} $^5D_0 \rightarrow {}^7F_2$ transition. This electric-dipole allowed transition is usually called as hypersensitive, so its intensity is strongly dependent on the Eu^{3+} surrounding, and it always will be dominant when Eu^{3+} is in the lattice site of noncentrosymmetric environment in the scheelite phases [20, 21]. The $^5D_0 \rightarrow {}^7F_1$ transition however has a magnetic dipole character and its intensity is almost independent of the environment. In this way, the ratio of the $(^5D_0 \rightarrow {}^7F_2)/(^5D_0 \rightarrow {}^7F_1)$ emission intensity, gave us valuable information about the symmetry of the site in which Eu^{3+} ions are situated [22]. It was not observed significant changes in the ratio of the $(^5D_0 \rightarrow {}^7F_2)/(^5D_0 \rightarrow {}^7F_1)$, which were of around 2.43 for the samples having Eu^{3+} concentrations from 0.01 to 0.075 mol, indicating that the Eu^{3+} surrounding in these samples is almost the same. The sample

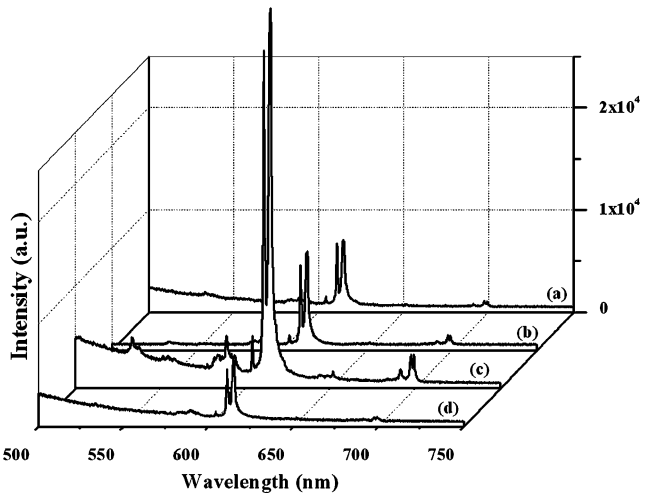

Fig. 4 Room-temperature emission spectra of the $Ba_{1-x}Eu_xMoO_4$ powders, where x=*a* 0.01, *b* 0.03, *c* 0.075 and *d* 0.145, heat-treated at 800 °C for 2 h, excited at 394 nm

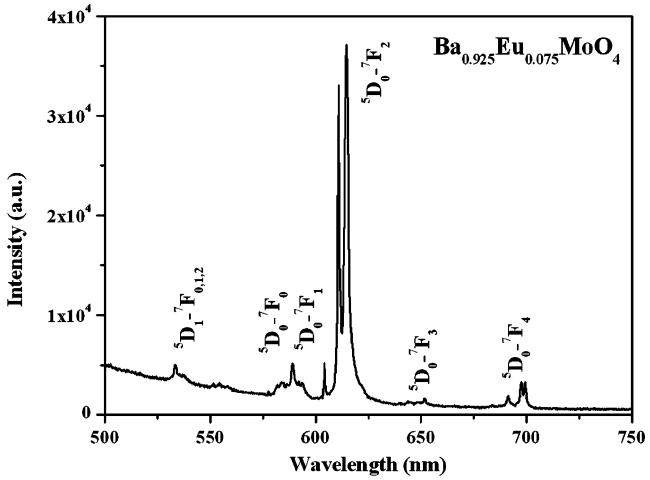

Fig. 5 Room-temperature emission spectra of the $Ba_{0.925}Eu_{0.075}MoO_4$ powder heat-treated at 800 °C, λ_{Exc}=394 nm

with 0.145 mol of Eu^{3+}, however, presents the ($^5D_0 \rightarrow {}^7F_2$)/($^5D_0 \rightarrow {}^7F_1$) ratio of 2.21, accusing an increase in the symmetry of the Eu^{3+} site.

The decay curves of the Eu^{3+} $^5D_0 \rightarrow {}^7F_2$ transition for the samples were obtained using the emission and excitation fixed at 614 and 394 nm, respectively. The decay times for BEMO samples having different Eu^{3+} concentrations were evaluated and it was not observed significant difference in its values, which was of around 0.54 ms. The decay curves followed the same one exponential behavior as already published for BEMO powders having 0.01 mol of Eu^{3+} heat treated at different temperatures [11].

Conclusion

$Ba_{1-x}Eu_xMoO_4$ (BEMO) powders, where x=0.0, 0.01, 0.03, 0.05, 0.075 and 0.145, heat treated at 800 °C for 2 h, was efficiently obtained in their crystalline scheelite-type phase by CPM in a small size grains and high morphological homogeneity. When the Eu^{+3} concentration in these powders increases, it was observed a broadening of the Bragg reflections and Raman bands, indicating an increase in the structural disorder of the material. It was also observed the presence of MoO_3 and $Eu_2Mo_2O_7$ as additional phases in the BEMO samples where the Eu^{3+} concentration was higher than 14.5 mol%. The Eu^{3+} doped samples presented the characteristic Eu^{3+} emissions of the $^5D_{0,1} \rightarrow {}^7F_{(0,1,2..)}$ transitions, being the most intense the $^5D_0 \rightarrow {}^7F_2$ one, located at 614 nm, originating the intrinsic Eu^{3+} red emission. The relative intensities of the Eu^{3+} emissions increase as the concentration of this ion increases from 0.01 to 0.075 mol, while in the $Ba_{0.855}Eu_{0.145}MoO_4$ sample the luminescence intensity was drastically quenched. The mechanism which prevails in this case is the energy transfer from one Eu^{3+} ion to another, which is responsible for the Eu^{3+} quenching concentration and the inhibition of its luminescence. The Eu^{3+} decay times of around 0.54 ms was evaluated from the monoexponential decay curves of the Eu^{3+} $^5D_0 \rightarrow {}^7F_2$ transition for the samples having different Eu^{3+} concentrations.

Acknowledgements FAPESP-CEPID, CNPq and CAPES.

References

1. Nathan MI, Nakamura S, Fasol G (1997) The blue laser diode. GaN based light emitters and lasers. Science 277(5322):46–47. doi:10.1126/science.277.5322.46b
2. Blasse G, Grabmeier BC (1994) Luminescent materials. Springer, Berlin
3. Shinoya M, Yen WM (1999) Phosphor handbook. CRC, Boca Raton
4. Silva CC, Filho FP, Sombra ASB, Rosa ILV, Leite ER, Longo E, Varela JA (2008) Study of structural and photoluminescent properties of $Ca_8Eu_2(PO_4)_6O_2$. J Fluoresc 18(2):253–259. doi:10.1007/s10895-007-0242-9
5. Morais EA, Scalvi LVA, Tabata A, De Oliveira JBB, Ribeiro SJL (2008) Photoluminescence of Eu^{3+} ion in SnO_2 obtained by sol–gel. J Mater Sci 43(1):345–349. doi:10.1007/s10853-007-1610-1
6. Blasse G, Bril A (1970) Characteristic luminescence. Philips Tech Rev 31(10):303–332
7. Ozuna O, Hirata GA, McKittrick J (2004) Luminescence enhancement in Eu^{3+}-doped alpha- and gamma-Al_2O_3 produced by pressure-assisted low-temperature combustion synthesis. Appl Phys Lett 84(8):1296–1298. doi:10.1063/1.1650908
8. Kiselev AP, Shmurak SZ, Red'kin BS, Sinitsyn VV, Shmyt'ko IM, Kudrenko EA, Ponyatovskii EG (2006) Evolution of the spectral response of amorphous europium molybdate under annealing. Phys Solid State 48(8):1544–1552. doi:10.1134/S1063783406080208
9. Canibano H, Boulon G, Palatella L, Guyot Y, Brenier A, Voda M, Balda R, Fernandez J (2003) Spectroscopic properties of new Yb^{3+}-doped $K_5Bi(MoO_4)_4$ crystals. J Lumin 102:318–326. doi:10.1016/S0022-2313(02)00526-4
10. Zhang ZJ, Chen HH, Yang XX, Zhao JT (2007) Preparation and luminescent properties of Eu^{3+} and Tb^{3+} ions in the host of $CaMoO_4$. Mater Sci Eng B 145(1–3):34–40. doi:10.1016/j.mseb.2007.09.091
11. Rosa ILV, Marques APA, Tanaka MTS, Melo DMA, Leite ER, Longo E, Varela JA (2008) Synthesis, characterization and photophysical properties of Eu^{3+} doped in $BaMoO_4$. J Fluoresc 18(2):239–245. doi:10.1007/s10895-007-0195-z
12. Maurera M, Souza AG, Soledade LEB, Pontes FM, Longo E, Leite ER, Varela JA (2004) Microstructural and optical characterization of $CaWO_4$ and $SrWO_4$ thin films prepared by a chemical solution method. Mater Lett 58(5):727–732. doi:10.1016/j.matlet.2003.07.002
13. Marques APD, de Melo DMA, Paskocimas CA, Pizani PS, Joya MR, Leite ER, Longo E (2006) Photoluminescent $BaMoO_4$ nanopowders prepared by complex polymerization method (CPM). J Solid State Chem 179(3):671–678. doi:10.1016/j.jssc.2005.11.020
14. Suryanarayana C, Norton MG (1998) X-ray diffraction: a practical approach. Plenum, New York
15. Basiev TT, Sobol AA, Voronko YK, Zverev PG (2000) Spontaneous Raman spectroscopy of tungstate and molybdate crystals for Raman lasers. Opt Mater 15(3):205–216. doi:10.1016/S0925-3467(00)00037-9
16. Moura MR, Ayala AP, Guedes I, Grimsditch M, Loong CK, Boatner LA (2004) Raman scattering study of $Tb(V_{1-x}P_x)O_4$ single crystals. J Appl Phys 95(3):1148–1151. doi:10.1063/1.1640461
17. Nakamoto K (1986) Infrared and Raman spectra of inorganic and coordination compounds, 4th. Wiley, New York
18. Hu YS, Zhuang WD, Ye HQ, Wang DH, Zhang SS, Huang XW (2005) A novel red phosphor for white light emitting diodes. J Alloy Comp 390(1–2):226–229. doi:10.1016/j.jallcom.2004.07.063
19. Marques APA, Picon FC, Melo DMA, Pizani PS, Leite ER, Varela JA, Longo E (2008) Effect of the order and disorder of $BaMoO_4$ powders in photoluminescent properties. J Fluoresc 18(1):51–59. doi:10.1007/s10895-007-0237-6
20. Sivakumar V, Varadaraju UV (2006) A promising orange-red phosphor under near UV excitation. Electrochem. Solid-State Lett 9(6):H35–H38. doi:10.1149/1.2189155
21. Gurmen E, Daniels E, King JS (1971) Crystal structure refinement of $SrMoO_4$, $SrWO_4$, $CaMoO_4$, and $BaWO_4$ by neutron diffraction. J Chem Phys 55(3):1093–1097. doi:10.1063/1.1676191
22. Rosa ILV, Maciel AP, Longo E, Leite ER, Varela JA (2006) Synthesis and photoluminescence study of $La_{1.8}Eu_{0.2}O_3$ coating on nanometric alpha-Al_2O_3. Mater Res Bull 41(10):1791–1797. doi:10.1016/j.materresbull.2006.03.026